ECS Transactions, 35 (1) 2409-2416 (2011)
10.1149/1.3570237 ©The Electrochemical Society

Chemical, Electronic and Nanostructure Dynamics on $Sr(Ti_{1-x}Fe_x)O_3$ Thin-Film Surfaces at High Temperatures

Yan Chen[a], Woo Chul Jung[b], Yener Kuru[a, b], Harry Tuller[b], and Bilge Yildiz[a]

[a] Department of Nuclear Science and Engineering, Massachusetts Institute of Technology Cambridge, Massachusetts 02139, USA
[b] Department of Materials Science and Engineering, Massachusetts Institute of Technology, Cambridge, Massachusetts 02139, USA

The surface structure, chemical composition and electronic structure of $Sr(Ti_{1-x}Fe_x)O_3$ under different temperatures and oxygen pressures were studied by Scanning Tunneling Microscopy / Spectroscopy (STM/S) and X-ray Photoelectron Spectroscopy (XPS). The surface structure remained stable to 430°C at 10^{-3} mbar oxygen pressure. When annealing at low oxygen pressure, the A to B site ratio, Sr/(Fe+Ti) decreased, Fe content at the B site increased, and particles that are likely to be Fe enriched, precipitated to the grain boundaries. Moreover, Fe changed its valence state, in part, from Fe^{3+} to Fe^{2+}, consistent with oxygen vacancy formation. The surface of STF was electrically insulating at room temperature, and exhibited by STS a well defined gap in the electronic density of states at 380°C. With further increase to 430°C, the energy gap disappeared. The variation in surface defects during thermal treatment is discussed as a likely reason for electronic structure changes at elevated temperatures.

Introduction

The slow oxygen reduction reaction (ORR) at the cathode is a major barrier to achieving high performance from solid oxide fuel cells (SOFC) at intermediate temperatures. Surface oxygen exchange and oxygen diffusion into the oxide cathodes are believed to be two key processes controlling ORR kinetics. While the electronic and ionic conductivity within the bulk of cathode materials is well studied, the relation of the surface activity to the surface structure, chemical composition and electronic structure remains unclear and controversial (1). Electrochemical investigation of porous electrodes is traditionally used to study the ORR kinetics, with kinetic parameters as reaction constants and energy barriers deduced (2). However, it remains a formidable challenge to isolate surface chemical and electronic properties from the electrochemical measurements on porous electrodes alone. More recently, dense thin film electrodes with simpler and more controlled geometries have enabled improved insight into the governing reaction pathways, the presence of surface segregation and of inhomogeneities in the electronic properties as function of surface microstructure (3-6). However, the harsh operating environments of the SOFC make it difficult to probe the surface chemical and electronic state *in situ* with conventional surface science techniques.

A key objective of this study is to identify how the electronic and chemical states of the dense thin film cathode surfaces evolve as a function of temperature and oxygen pressure. For this purpose, we use a modified scanning tunneling microscope that enables topographic imaging and electronic structure characterization with high spatial resolution at elevated temperatures and in an oxygen environment. The broader impact of our work is expected to enable the correlation of surface structure, electron tunneling and chemical characteristics to the oxygen reduction kinetics at the atomistic level on SOFC cathode surfaces.

The material we chose to study is the $Sr(Ti_{1-x}Fe_x)O_3$ (STF) solid solution system, which is stable over a wide range of temperature and oxygen pressures (P_{O2}). The capability of adjusting its ionic and electronic conductivity over wide limits via variations in the Fe content make it an ideal model material for study (7). The defect chemistry and bulk conductivity of STF are well studied (8, 9) and importantly, the oxygen exchange process at the surface was indentified to be the rate limiting step (10, 11).

Experimental Approach

$SrTi_{0.65}Fe_{0.35}O_3$ (STF) dense thin films with thickness of 130 nm were grown by pulsed laser deposition (PLD) onto (100) oriented single crystal yttria doped zirconia (YSZ) substrates (MTI Corporation, Richmond, CA). The film was confirmed by XRD to be highly textured along the (110) out of plane direction. High spatial resolution probing of the surface structure and electronic state was achieved via *in situ* Scanning Tunneling Microscopy and Spectroscopy (STM, STS) at high temperature and O_2 environment (Omicron GmbH). The oxygen doser was placed near the STM stage in the chamber to achieve higher oxygen pressure at the sample surface. Samples were radiatively heated by a pyrolytic boron nitride (PBN) heater for cleaning the sample and for high temperature measurements. X-ray Photoelectron Spectroscopy (XPS), within the same chamber, was used to identify the chemical state of the surface before and after the STM/STS measurements. Mg X-ray source of 1253.6 eV, at a power of 300W, was used for XPS measurements. This combined set-up avoids contamination of the surface in sample transfer between the XPS and STM/STS measurements.

Results and Discussion

Surface Structure

The film surface topography, electronic structure, and chemistry exhibited temperature- and oxygen partial pressure-dependent characteristics. At room temperature, the STF films were insulating. At temperatures near 300^{o}C, the films had sufficient concentration of free carriers to enable STM/STS measurements. The morphology of the surface is shown in Fig. 1-a. The film exhibits grain sizes of 20 to 30 nm. At temperatures up to 430^{o}C, the surface topography remains stable in oxygen pressures of 10^{-3} mbar. When the pressure decreased to 10^{-9} mbar, additional particles precipitate at the surface, preferentially at the grain boundaries, as shown in Fig. 1-b.

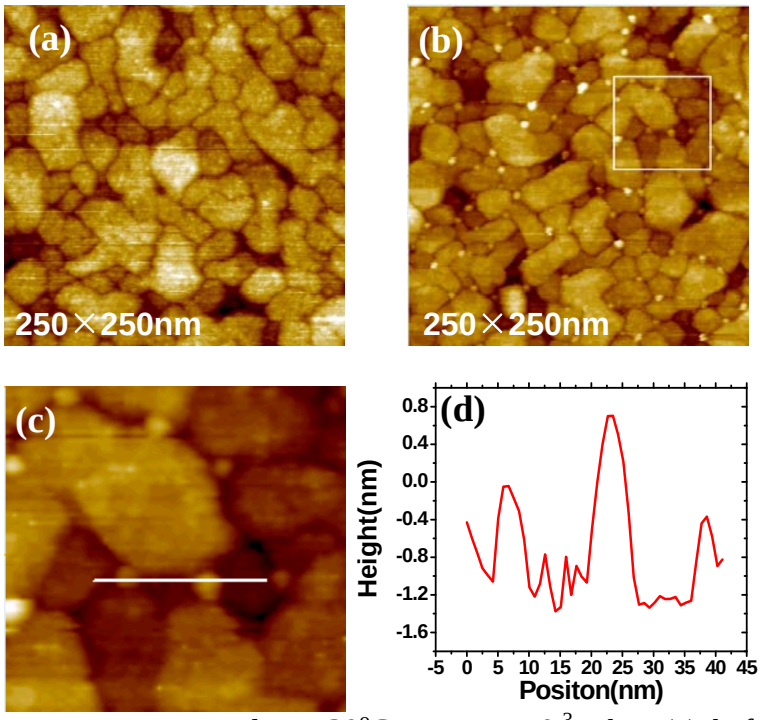

Figure 1. STM image measured at 430°C, P_{O2}~ 1×10^{-3} mbar (a) before and (b) after annealing at 1×10^{-10} mbar; (c) Boxed part of the image in (b), zoomed in; (d) height profile from (c).

Chemical Composition

The surface was found to be enriched in the A site cation (Sr) content in its as-prepared state. The A to B site ratio, Sr/(Ti+Fe), was about 2.1. The Fe content at the B site was 34%, close to the bulk value. To avoid the impact of surface contamination on the interpretation of surface composition changes, the film was first heated to 430°C in 10^{-3} mbar oxygen for 2 hours to clean the surface of carbon contamination. After this cleaning procedure, the carbon content at the surface was less than 5%. Below we discuss changes in the surface cation content and chemical states as a function of oxygen partial pressure.

1) Surface Cation Content: As shown in Fig. 2-a, when the oxygen pressure decreases from 10^{-3} mbar to 10^{-9} mbar, the A to B site ratio (Sr/(Ti+Fe)) decreases and the Fe content at the B site increases. Fig. 2-b shows the relative fraction of each cation as a function of oxygen pressure. We can see that annealing at lower oxygen pressures causes Fe to increase at the surface and for Sr to decrease, while Ti remains unchanged. The changes as a function of pressure are only partially reversible.

The changes observed for the Sr/(Ti+Fe) ratio as function of O_2 pressure is in agreement with previous observations for $SrTiO_3$ (STO) upon thermal treatment: for reduced STO, the B site (Ti) was found to segregate to the surface, while for oxidized STO the surface was enriched with Sr (12-16). The work of Szot and Speier et al. (12, 13) suggested that the chemical composition change on STO upon thermal treatment could be associated with the redistribution of Sr and/or SrO. They proposed that when STO is reduced, the surface is depleted of Sr and O, and the TiO_2 layer can be exposed. At the same time, oxygen vacancies were created. In our work, we observed the decrease of A

site content when STF was heated in low oxygen pressure at 430°C, which was much lower than the temperature used in other reported work, mostly above 900°C (12-16). However, it is known that the Sr mobility is already significant in perovskites at temperature as low as 300°C (17). Moreover, the high grain boundary density of our nano-crystalline STF films can serve as fast diffusion paths for a redistribution of the cations, predominantly of Sr, in the near-surface region. It is possible that the decrease of the Sr surface content observed in this study at low oxygen pressure was the result of the movement of Sr from the surface into the bulk STF.

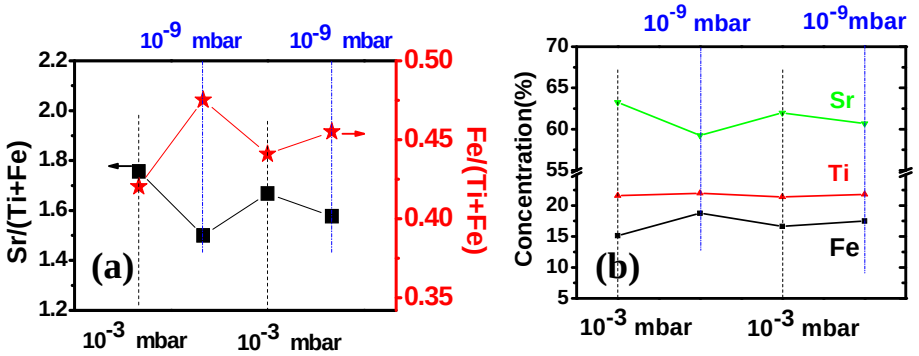

Figure 2. Chemical composition under different oxygen pressures at 430°C (a) A to B site ratio Sr/(Fe+Ti) and Fe concentration at B site, Fe/(Fe+Ti); (b) Relative concentration of each cation at the surface.

We note that the Fe increase observed in XPS occurs at the same conditions as the particle precipitation at the boundaries shown by STM. It is possible that surface segregated Fe prefers to precipitate at the grain boundary as an iron enriched phase. In acceptor doped $SrTiO_3$, segregation of dopants to the grain boundaries is generally observed and is considered to play an essential role in determining the electronic properties of the film (18-21). In the work by Wang et al., metallic Fe particles were found at grain boundaries and triple junctions in bulk Fe-doped $SrTiO_3$ by heating to 1350°C in H_2 (20). The conditions examined here are not nearly as reducing as reported in refs 19-21. However, surface segregation and precipitation may begin under less reducing conditions than those required for phase separation in bulk microcrystalline STF. While the driving force for Fe segregation to the surface remains to be determined, *ab initio* calculations by Alexandrov et al. (22) do find that the energy for substituting Ti with Fe is lower at the surface than in the bulk for Fe doped $SrTiO_3$. But whether heating STF in reducing environment could promote such tendency still needs more work to confirm.

2) Cation Chemical States: The Fe 2p, Ti 2p and Sr 3d peaks from the x-ray photoelectron spectra at different oxygen pressures are shown in Fig. 3. The peak position is calibrated with respect to the lattice oxygen peak at 528.9 eV. At 1×10^{-3} mbar, Fe $2p_{1/2}$ and $2p_{3/2}$ are at 723.2 eV and 709.7 eV respectively. Fe 2p shows an apparent satellite peak at 718.1 eV, corresponding to the presence of Fe^{3+} (23-25). The satellite peak disappears upon reducing the oxygen pressure to 1×10^{-9} mbar. This indicates that the valence state of Fe reduces to a mixed state of Fe^{3+} and Fe^{2+} (23-25). The increase of FWHM for the $2p_{3/2}$ peak from 2.4 eV to 2.7 eV is another indication of the mixed valance state of Fe (25). The Fe peak shifts slightly to lower binding energy, 722.7 eV for Fe $2p_{1/2}$ and 709.2eV for Fe $2p_{3/2}$. This change in peak position is caused by the increase of Fe^{2+} content, which has a lower binding energy compared to Fe^{3+}. The evident

change in the Fe reduction state from Fe^{3+} to Fe^{2+} suggests the corresponding formation of oxygen vacancies on the surface. No evidence for metallic Fe is observed on the surface. In bulk Fe-doped STO, Fe^{2+} is observed only when heated to temperatures above 1000°C (26); the presence Fe^{2+} is observed at much lower temperatures at the surface of our STF films. This suggests that the oxygen vacancy formation energy on the surface may be much lower than that in the bulk of STF.

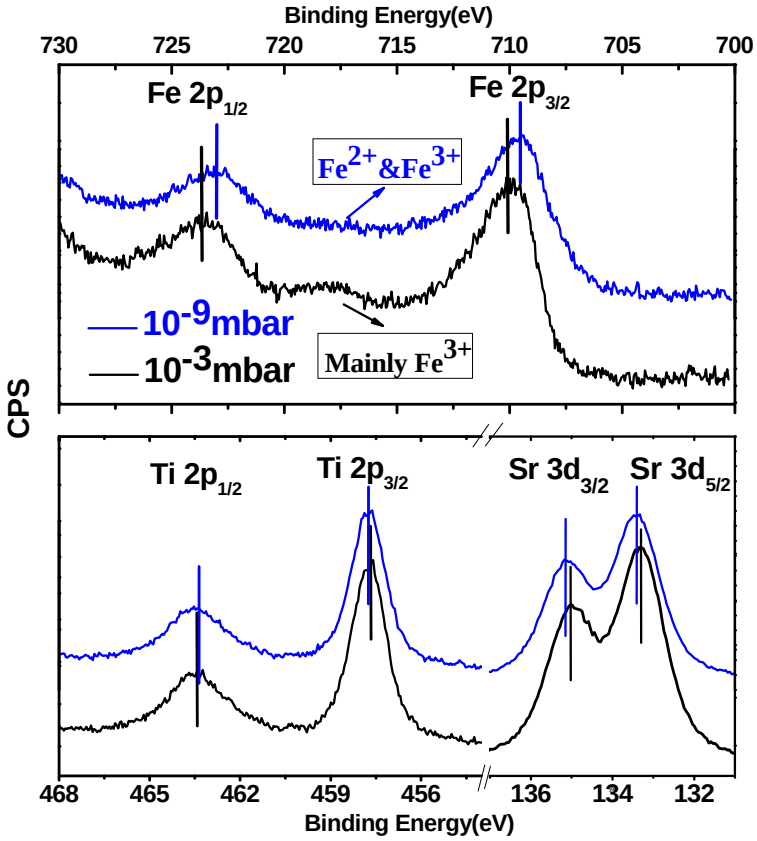

Figure 3. Comparison of Fe 2p, Ti 2p and Sr 3d x-ray photoemission peaks upon annealing at 10^{-3} and at 10^{-9} mbar.

As shown in Fig. 3, the Ti $2p_{1/2}$ and $2p_{3/2}$ peaks are at 463.4 eV and 457.7 eV with a separation of 5.7 eV, in agreement with the XPS results for Ti^{4+} (24, 27). Sr 3d doublet spectra are fit to two peaks, the ratio between the Sr $3d_{3/2}$ and $3d_{5/2}$ peak areas being close to 2:3 which is the theoretical value. At 10^{-3} mbar, Sr $3d_{3/2}$ and $3d_{5/2}$ peaks are at 135.1 and 133.3 eV, as reported for Sr^{2+} of STO (24, 27). No apparent changes in peak position and peak shape were observed at different oxygen pressures for Sr and Ti. This indicates that the valence states of Ti and Sr do not change within our detection limits.

In summary, we identified that STF exhibits oxygen pressure dependent changes in its surface cation content and chemistry. These changes favor a decrease in A site to B site ratio at lower oxygen pressures, accompanied by an increase in the Fe content on the B site. Furthermore, Fe in part reduces from Fe^{3+} to Fe^{2+} on the surface at relatively low temperatures of 430°C. The decrease of Sr content at the surface could be related to the Sr movement into the subsurface, which was also observed on STO under significantly reducing environments (12, 13). The difference in the formation energy of Fe substitution at the surface and in the bulk could be one possible driving force that induced the segregation of Fe to the surface at lower oxygen pressures. Based on our observation

of the segregation of Fe to the surface, we hypothesize that the particles that formed at the grain boundaries may be an iron-enriched phase.

Surface Electronic Structure

Tunneling spectroscopy shows that the electronic structure of the surface strongly depends on the environment to which the film is subjected. At room temperature, the surface is insulating and the film needs to be taken to higher temperatures to enable STM/STS measurements. The average tunneling spectra at 380°C (Fig. 4) exhibits an energy gap in the density of electronic states (DOS) near the Fermi level (0 V). At this temperature, three characteristic band gap values, around 1.2 eV, 1.6 eV and 2.5 eV were observed. Upon heating to 430°C, no remaining gap in the DOS was observed. This suggests the possibility that initially localized carriers become delocalized and/or the increasing formation of oxygen vacancies release increasing levels of carriers at elevated temperatures. More studies are required to clarify these observations.

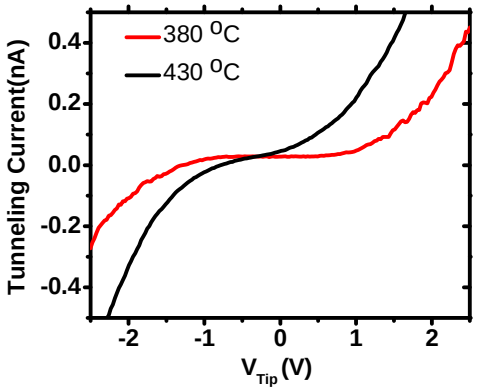

Figure 4. Tunneling spectra measured at 380 and 430°C, P_{O2}~ 10^{-3}mbar (V_{tip} = 2 V, I = 500 pA)

For bulk $SrTi_{0.65}Fe_{0.35}O_3$, the band gap is reported to be ~ 2.5 eV (7). In this study, several band gap values were observed at the surface including one equal to the bulk value. The variation in band gap values could be associated with the presence of localized defects on the surface. The formation of oxygen vacancies modify the *d* band structure of the neighboring transition metals and can induce states in the gap (28). The formation of oxygen vacancies on TiO_2 – terminated surfaces of STO was reported to create a band within the energy gap (29, 30). Beyond single oxygen vacancies, defect clusters like cation-oxygen vacancy complexes can also impact the local surface electronic structure. One example can be found in the ab initio calculations of Kim *et al.* (31) for the cluster of a Sr vacancy and two oxygen vacancies which is reported to induce a defect band with a gap of 1.3 eV. This is consistent with the observation in this study of a reduction in Sr content and the generation of oxygen vacancies at elevated temperatures on STF surfaces. While these may serve as possible governing mechanisms in the temperature dependent transitions in electronic structure, the exact mechanism still requires further investigation.

Conclusions

The surface electronic, chemical, and topographic behavior of highly textured $SrTi_{0.65}Fe_{0.35}O_3$ thin films varied significantly as a function of temperature and oxygen

partial pressure. Structurally, particles, likely to be Fe-enriched secondary phases, were identified at the grain boundaries when the film was reduced at 430°C and 10^{-9} mbar. Chemically, the A to B site ratio was found to decrease and the Fe content to increase with decreasing oxygen pressure. Fe was also found to partially reduce its valance state to Fe^{2+}. Electronically, the surface changed from insulating, to semiconducting (energy gap) to metallic (zero gap) with increasing temperature. This may be related to the formation of oxygen vacancies and Fe^{2+} during the annealing process. These results represent an initial set of *in situ* surface structure, chemical composition and electronic state correlations on dense thin film STF model cathodes as a function of the environment. In depth analysis of such correlations are essential towards advancing our understanding of how the surface condition relates to the oxygen reduction activity on SOFC cathodes.

Acknowledgements

The authors acknowledge the U.S.-DOE Basic Energy Sciences, Grant No. DE-SC0002633 for financial support, and thank Z. Cai, H. Jalili for help with measurements and analysis, and J. J. Kim for help with sample preparation.

References

1. S. B. Adler, *Chem. Rev.*, **104**, 4791 (2004).
2. J. VanHerle, A. J. McEvoy and K. R. Thampi, *Electrochim. Acta*, **41**, 1447 (1996).
3. F. S. Baumann, J. Fleig, M. Konuma, U. Starke, H. U. Habermeier and J. Maier, *J. Electrochem. Soc.*, **152**, A2074 (2005).
4. G. J. la O', B. Yildiz, S. McEuen and Y. Shao-Horn, *J. Electrochem. Soc.*, **154**, B427 (2007).
5. R. A. De Souza, *Phys. Chem. Chem. Phys.*, **8**, 890 (2006).
6. J. Fleig, R. Merkle and J. Maier, *Phys. Chem. Chem. Phys.*, **9**, 2713 (2007).
7. A. Rothschild, W. Menesklou, H. L. Tuller and E. Ivers-Tiffee, *Chem. Mater*, **18**, 3651 (2006).
8. R. Merkle and J. Maier, *Phys. Chem. Chem. Phy.*, **4**, 4140 (2002).
9. V. E. Alexandrov, J. Maier and R. A. Evarestov, *Phys. Rev. B*, **77**, 9 (2008).
10. W. Jung and H. L. Tuller, *Solid State Ion.*, **180**, 843 (2009).
11. W. Jung and H. L. Tuller, *J. Electrochem. Soc.*, **155**, B1194 (2008).
12. K. Szot, W. Speier, J. Herion and C. Freiburg, *Appl. Phys. A-Mater. Sci. Process.*, **64**, 55 (1997).
13. K. Szot and W. Speier, *Phys. Rev. B*, **60**, 5909 (1999).
14. P. A. W. van der Heide, Q. D. Jiang, Y. S. Kim and J. W. Rabalais, *Surf. Sci.*, **473**, 59 (2001).
15. H. Wei, L. Beuermann, J. Helmbold, G. Borchardt, V. Kempter, G. Lilienkamp and W. Maus-Friedrichs, *J. European Ceram. Soc.*, **21**, 1677 (2001).
16. A. Gunhold, L. Beuermann, K. Gomann, G. Borchardt, V. Kempter, W. Maus-Friedrichs, S. Piskunov, E. A. Kotomin and S. Dorfman, *Surf. Interface Anal.*, **35**, 998 (2003).
17. H. W. Nesbitt, G. M. Bancroft, W. S. Fyfe, S. N. Karkhanis and A. Nishijima, *Nature*, **289**, 358 (1981).
18. I. Denk, J. Claus and J. Maier, *J. Electrochem. Soc.*, **144**, 3526 (1997).

19. S. M. Wang and S. J. L. Kang, *Appl. Phys. Lett.*, **89**, 3 (2006).
20. S. M. Wang and S. J. L. Kang, *J. Am. Ceram. Soc.*, **91**, 2617 (2008).
21. V. Ravikumar, R. P. Rodrigues and V. P. Dravid, *J. Phys. D-Appl. Phys.*, **29**, 1799 (1996).
22. V. E. Alexandrov, R. A. Evarestov, E. A. Kotomin and J. Maier, in *Ab Initio Simulation of Crystalline Solids: History and Prospects - Contributions in Honor of Cesare Pisani*, R. Dovesi, R. Orlando and C. Roetti Editors, p. 12001, Iop Publishing Ltd, Bristol (2008).
23. T. C. Lin, G. Seshadri and J. A. Kelber, *Appl. Surf. Sci.*, **119**, 83 (1997).
24. J. F. Moulder and J. Chastain, *Handbook of x-ray photoelectron spectroscopy : a reference book of standard spectra for identification and interpretation of XPS data*, p. 261 p., Physical Electronics Division, Perkin-Elmer Corp., Eden Prairie, Minn. (1992).
25. S. Gota, E. Guiot, M. Henriot and M. Gautier-Soyer, *Phys. Rev. B*, **60**, 14387 (1999).
26. V. G. Bhide and H. C. Bhasin, *Physical Review*, **172**, 290 (1968).
27. P. V. Nagarkar, P. C. Searson and F. D. Gealy, *J. Appl. Phys.*, **69**, 459 (1991).
28. M. V. Ganduglia-Pirovano, A. Hofmann and J. Sauer, *Surf. Sci. Rep.*, **62**, 219 (2007).
29. T. Nishimura, A. Ikeda, H. Namba, T. Morishita and Y. Kido, *Surf. Sci.*, **421**, 273 (1999).
30. A. Hirata, A. Ando, K. Saiki and A. Koma, *Surf. Sci.*, **310**, 89 (1994).
31. Y. S. Kim, J. Kim, S. J. Moon, W. S. Choi, Y. J. Chang, J. G. Yoon, J. Yu, J. S. Chung and T. W. Noh, *Appl. Phys. Lett.*, **94**, 3 (2009).